A Surface PEEC Formulation for High-Fidelity Analysis of the Current Return Networks in Composite Aircrafts

Mauro Bandinelli, Alessandro Mori, Giovanni Galgani, Daniele Romano, Giulio Antonini, *Senior Member, IEEE*, Anca-Lucia Goleanu Dieudonné, and Michel Dunand

***Abstract*—This paper describes the approach developed to model the current return networks installed aboard aircrafts having parts made in composite materials. The surface partial element equivalent circuit (PEEC) method is adopted for its high-fidelity modeling capabilities, and its accuracy in the low-frequency region, which is of interest for the characterization of the return networks. State of the art of PEEC modeling is implemented in order to allow real-life aircrafts to be modeled. A special complex mock-up has been realized and measured. The numerical results are compared with measurements to assess their adequacy.**

***Index Terms*—Almost equipotential electrical network, composite aircrafts, current return network, partial element equivalent circuit (PEEC) method.**

I. Introduction

THE metallic bodies of "standard" aircrafts are commonly used as conductive electrical pathways for the return of direct and alternating currents, faults currents, lightning currents, and also other functions related to voltage differentials, electrostatic charge draining, electromagnetic shielding, etc.

The low conductivity and the high thermal sensitivity of new composite materials used for aircraft skin and structures no more allow this. The functions of the previous metallic structure have to be taken by a dedicated conductive electrical network, added into the aircraft body. This network is hereby called "almost equipotential electrical network" (ALEEN). This network is composed of the metallic and/or composite skin, composite, or metallic structural elements, such as frames, crossbeams, rails, etc., and also of dedicated paths, protection sleeves, raceways, conductive wires, etc. This new network is not an ideal ground and shows a lower measurable performance than those currently obtained on metal aircrafts.

Manuscript received June 16, 2014; revised December 30, 2014; accepted March 14, 2015. This work was supported by the European Commission under Grant 296536.

M. Bandinelli, A. Mori, and G. Galgani are with Ingegneria dei Sistemi (IDS), 56121 Pisa, Italy (e-mail: m.bandinelli@idscorporation.com; a.mori@idscorporation.com; g.galgani@idscorporation.com).

D. Romano and G. Antonini are with the Department of Industrial and Information Engineering and Economics, University of L'Aquila, 67100 L'Aquila, Italy (e-mail: daniele.romano.vis@gmail.com; giulio.antonini@univaq.it).

A. L. Goleanu Dieudonné and M. Dunand are with the EWIS R&T Department of Labinal Power Systems, SAFRAN Group, 31700 Blagnac, France (e-mail: anca.dieudonne@labinal-power.com; michel.dunand@labinal-power.com).

Color versions of one or more of the figures in this paper are available online at http://ieeexplore.ieee.org.

Digital Object Identifier 10.1109/TEMC.2015.2422672

Aeronautical manufacturers and providers of cable harness and equipment are interested in having an accurate electrical/electromagnetic characterization of a given ALEEN configuration, in order to be able to correctly design the electrical wiring interconnection system (EWIS), thus reducing design margins and saving mass. Further, such main actors and also certification authorities can be interested to estimate how the selected ALEEN configuration works with respect to other required functions (e.g., faults currents, lightning currents, electromagnetic shielding, etc.) and eventually to optimize it without needing expensive (and sometime almost unfeasible) repeated bread boarding.

Clean Sky is a public private partnership between the European Commission and the Aeronautical Industry and was set up to bring significant step changes regarding the environmental impact of aviation. In the framework of Clean Sky–Systems for Green Operations (SGO), the project GENIAL was launched. This project, led by Labinal–SAFRAN Group, world leader in providing EWIS solutions for aeronautics, aimed at developing a numerical methodology and a Computer Aided Engineering (CAE) tool [29] suited to model the current return networks installed aboard aircrafts. The tool is able:

1) to input ALEEN geometries and material properties and EWIS pathways from CAD;
2) to evaluate the equivalent impedance matrix of ALEEN (i.e., among any couple of ALEEN terminals where a terminal represents the connection point of a load or a source to the ALEEN network) in the frequency range dc–MHz, also considering the EWIS pathways and the electromagnetic interaction with aircraft body;
3) to interface the aforementioned impedance matrix with an electrical database of EWIS, in order to allow correct calculation and technological design of the circuit impedance between any two interconnection points of EWIS;
4) to visualize induced current and voltage distribution on the aircraft/ALEEN.

Full-wave three-dimensional (3-D) modeling based on the partial element equivalent circuit (PEEC) method is applied, in which all the electromagnetic interactions are considered (capacitive and inductive mutual coupling, skin and proximity effects, etc.).

The PEEC method [1]–[3] is derived from Maxwell's equations and can be used to model the electromagnetic behavior of arbitrary 3-D electrical structures. Such a methodology has been selected for its effectiveness in the low-frequency region (where

the well-known "low-frequency break-down effect" makes the problem ill-conditioned). Due to the tight requirements in terms of accuracy (milliohms range was required on impedance values between any two points on ALEEN), particular effort has been devoted to pursue the concept of "high-fidelity modeling," not requiring the user to simplify the numerical model with respect to the CAD model. Acceleration methods can be used in order to allow a significant reduction of the hardware resources in analysis of large structures.

The low-frequency break-down effect of electric field integral equation (EFIE) can be mitigated also by using, in classical method of moments, a loop-tree decomposition or the multiresolution (MR) approach [4], [5]. In particular, the MR mitigates also the ill conditioning due to a multiscale geometry (i.e., due to the presence of strongly nonuniform mesh elements). However, such approaches result in a more complex implementation respect to the PEEC method.

This paper describes the mathematical details and the implementation of the surface PEEC formulation employed and its validation by means of an extensive experimental measurement campaign performed on a mock-up realized by Labinal. The mock-up was designed and built to well represent real aircraft configurations, resulting in an unprecedented complicated structure to analyze with computer codes.

II. PEEC Theory Review

PEEC models have been used extensively to describe discrete approximations of the EFIE in relation to the electromagnetic analysis of interconnect, packaging structures, and power systems. The PEEC method is basically an EFIE-based approach that provides an equivalent circuit of the EFIE in terms of the capacitive and inductive interactions between the elemental currents and charges in the discretized structure [3], [10]. Over the years, many improvements have been done with respect to the original formulation, including nonorthogonal geometries [8], [12], dielectric and magnetic material modeling [6], [7], [11], more efficient solvers [9], [13]–[16], [19]–[21], and parameterized models [17], [18], [22], [23].

The degrees of freedom in the PEEC formulation are represented by the electric currents, charges, and potentials (voltages), quantities that are appropriate for an equivalent circuit representation. At any point in a conductor, the EFIE in the frequency domain reads

$$\boldsymbol{E}_0(\boldsymbol{r},\omega) = \frac{\boldsymbol{J}(\boldsymbol{r},\omega)}{\gamma} + j\omega\frac{\mu_0}{4\pi}\int_V \frac{\boldsymbol{J}(\boldsymbol{r}',\omega)\,e^{-jk|r-r'|}}{|\boldsymbol{r}-\boldsymbol{r}'|}dV' + \nabla\boldsymbol{\Phi}(\boldsymbol{r},\omega) \tag{1}$$

where γ represents the electrical conductivity of conductors, $\boldsymbol{J}(\boldsymbol{r},\omega)$ the volumetric current density, $\boldsymbol{\Phi}(\boldsymbol{r},\omega)$ the electric scalar potential, $\boldsymbol{E}_0(\boldsymbol{r},\omega)$ the incident electric field radiated by external sources, and $k=\omega/c_0$ is the wavenumber. Assuming the charge to be located on the surface of conductors, the electric scalar potential is related to the charge distribution by

$$\boldsymbol{\Phi}(\boldsymbol{r},\omega) = \frac{1}{4\pi\varepsilon_0}\int_{S'}\frac{\sigma(\boldsymbol{r}',\omega)\,e^{-jk|\boldsymbol{r}-\boldsymbol{r}'|}}{|\boldsymbol{r}-\boldsymbol{r}'|}dS' \tag{2}$$

where $\sigma(\boldsymbol{r}',\omega)$ is the surface density charge.

In PEEC modeling, in addition to the EFIE, the continuity equation is enforced. It reads

$$\nabla\cdot\boldsymbol{J}(\boldsymbol{r},\omega) = 0 \quad \text{in volumes} \tag{3a}$$

$$\hat{\boldsymbol{n}}\cdot\boldsymbol{J}(\boldsymbol{r},\omega) = j\omega\sigma(\boldsymbol{r},\omega) \quad \text{on surfaces.} \tag{3b}$$

In the classical PEEC formulation, in order to obtain a system of equations, volumes are usually discretized in hexahedra and surfaces in quadrilaterals. If dielectrics are to be modelled, volumetric polarization currents are considered [6], [7].

One standard numerical procedure for solving (1)–(3a) and (3b) begins with approximating the volume currents and surface charges by a weighted sum of a finite set of basis functions $\boldsymbol{f}_n(\boldsymbol{r})$ and $g_k(\boldsymbol{r})$ as in

$$\boldsymbol{J}(\boldsymbol{r},\omega) = \sum_{n=1}^{N_v} I_n(\omega)\,\boldsymbol{f}_n(\boldsymbol{r}) \tag{4a}$$

$$\sigma(\boldsymbol{r},\omega) = \sum_{k=1}^{N_s} q_k(\omega)\,g_k(\boldsymbol{r}). \tag{4b}$$

Following the standard Galerkin's testing procedure, topological elements, namely nodes and branches are generated and electrical lumped elements are identified modeling both the magnetic, the electric field coupling and the losses. Applying the standard Galerkin's testing procedure to (1), we obtain

$$-\boldsymbol{A}\Phi - \boldsymbol{R}\boldsymbol{I} - j\omega\boldsymbol{L}p\boldsymbol{I} = \boldsymbol{V}_s \tag{5}$$

where matrix $\boldsymbol{A}$ represents the connectivity matrix, relating nodes, and branches of the PEEC equivalent circuit, $\boldsymbol{R}$ is a diagonal matrix containing the resistances of each elementary hexahedron, $\boldsymbol{L}p$ is the matrix of partial inductances describing the magnetic field coupling, and $\boldsymbol{V}_s$ represents both longitudinal voltage sources reproducing the distributed effect of incident fields and eventually lumped voltage sources. It can be regarded as Kirchhoff voltage law (KVL) enforced to the equivalent circuit. Applying the Galerkin's testing procedure to (2) yields

$$\boldsymbol{\Phi} = \boldsymbol{P}\boldsymbol{Q} \tag{6}$$

where $\boldsymbol{P}$ is the matrix of coefficient of potentials, describing the electric field coupling among elementary quadrilaterals.

Finally, the continuity equations (3a) and (3b) are to be enforced. Integrating (3a) over the elementary volume cells and (3b) over the elementary surface cells, (3a) and (3b) can be written in a compact form as

$$j\omega\boldsymbol{Q} - \boldsymbol{A}^t\boldsymbol{I} = \boldsymbol{0}. \tag{7}$$

If lumped elements and external currents sources are connected to surface nodes, (7) becomes

$$j\omega\boldsymbol{Q} + \boldsymbol{Y}_{le}\boldsymbol{\Phi} - \boldsymbol{A}^t\boldsymbol{I} = \boldsymbol{I}_s \tag{8}$$

where $\boldsymbol{Y}_{le}$ is the admittance matrix of lumped elements and $\boldsymbol{I}_s$ is a vector containing the external currents injected into the nodes. (7) and (8) can be regarded as Kirchhoff current laws enforced to the equivalent circuit.

Upon substitution of (6) into (8), we obtain

$$j\omega \boldsymbol{P}^{-1}\boldsymbol{\Phi} + \boldsymbol{Y}_{le}\boldsymbol{\Phi} - \boldsymbol{A}^t\boldsymbol{I} = \boldsymbol{I}_s \tag{9}$$

which can be recast as

$$j\omega\boldsymbol{\Phi} + \boldsymbol{P}\boldsymbol{Y}_{le}\boldsymbol{\Phi} - \boldsymbol{P}\boldsymbol{A}^t\boldsymbol{I} = \boldsymbol{P}\boldsymbol{I}_s. \tag{10}$$

Finally, the set of equations to be solved are

$$\begin{bmatrix} -\boldsymbol{A} & -(\boldsymbol{R} + j\omega\boldsymbol{L}p) \\ j\omega\boldsymbol{U} + \boldsymbol{P}\boldsymbol{Y}_{le} & -\boldsymbol{P}\boldsymbol{A}^t \end{bmatrix} \begin{bmatrix} \boldsymbol{\Phi} \\ \boldsymbol{I} \end{bmatrix} = \begin{bmatrix} \boldsymbol{V}_s \\ \boldsymbol{P}\boldsymbol{I}_s \end{bmatrix} \tag{11}$$

where $\boldsymbol{U}$ is the identity matrix. $\boldsymbol{A}$ and $\boldsymbol{Y}_{le}$ are sparse matrices, $\boldsymbol{R}$ is a diagonal matrix,[1] and $\boldsymbol{L}p$ and $\boldsymbol{P}$ are dense matrices.

In the frequency range of interest, these matrices can contain elements having a very large (or very tiny) modulus. This can lead to numerical inaccuracies, especially in case an iterative solver is used. (11) can be regarded as obtained applying the modified nodal analysis (MNA) [22] to the equivalent circuit generated by the PEEC method.

It is worth pointing out that the low-frequency solution of integral equation based techniques is typically an ill-conditioned problem. The PEEC solution (11) alleviates such a problem by keeping separate the magnetic and electric field contributions to the EFIE, by using the MNA.

A. Surface Modeling in PEEC Algorithm Through the Use of RWG Basis Functions

The classical PEEC method relies on an orthogonal discretization of all structures using, for example, parallelepipeds as elementary volumes and rectangles as elementary surfaces. This paradigm, which assumes a dominant direction of current flow along the length of conductors, is well suited for interconnect structures. Whenever the scenario involves some arbitrarily shaped structures, the direction of currents is substantially arbitrary.

In this perspective, if only the surfaces of conductors are discretized, Rao–Wilton–Glisson (RWG) basis functions [25]—which are linear basis functions defined over triangles—can be used to model conductors using surface triangular meshes.

As discussed in the previous section, the PEEC formulation is based on the enforcement of a discrete approximation of the equation for the electric field intensity which, on the conductor surface, results in the following surface integral equation statement of the electromagnetic boundary problem

$$Z_s^{\text{eff}}(\boldsymbol{r})\,\boldsymbol{J}_s(\boldsymbol{r}) + \frac{j\omega\mu_0}{4\pi}\iint_{S_c} G_0(\boldsymbol{r},\boldsymbol{r}')\boldsymbol{J}_s(\boldsymbol{r}')ds' + \frac{1}{4\pi\varepsilon_0}\nabla\iint_{S_c} G_0(\boldsymbol{r},\boldsymbol{r}')\sigma(\boldsymbol{r}')ds' = \boldsymbol{E}_0(\boldsymbol{r}) \tag{12}$$

where S_c denotes all metallization surfaces and $Z_s^{\text{eff}}(\boldsymbol{r})$ is the effective surface impedance, which relates the tangential components of the electric and magnetic field vector on the conductor surface. Also, the well-known resistive and skin effects are considered into $Z_s^{\text{eff}}(\boldsymbol{r})$. Thus, assuming that the unit normal $\hat{\boldsymbol{n}}$ to the conductor forms with the unit tangents $\hat{\boldsymbol{t}}_1$ and $\hat{\boldsymbol{t}}_2$ a right-handed system at each point on the conductor surface the surface impedance condition assumes the form

$$E_{t1}(\boldsymbol{r})\,\hat{\boldsymbol{t}}_1 + E_{t2}(r)\,\hat{\boldsymbol{t}}_2 = Z_s^{\text{eff}}(\boldsymbol{r})\,\hat{\boldsymbol{n}} \times \boldsymbol{H}(\boldsymbol{r}). \tag{13}$$

The way $Z_s^{\text{eff}}(\boldsymbol{r})$ can be calculated is discussed in the following. In the following, we will refer to this formulation of PEEC method as surface PEEC (S-PEEC) formulation.

The discrete statement obtained from Galerkin's testing (12) using RWG expansion functions and taking (5) into account, is then cast in the following form:

$$-\boldsymbol{A}\boldsymbol{\Phi} - \left(\hat{\boldsymbol{Z}} + j\omega\boldsymbol{L}p\right)\boldsymbol{I} = \boldsymbol{V}_s. \tag{14}$$

In addition to (14), as before, the continuity equation is to be enforced as:

$$j\omega\boldsymbol{\Phi} + \boldsymbol{P}\boldsymbol{Y}_{le}\boldsymbol{\Phi} - \boldsymbol{P}\boldsymbol{A}^t\boldsymbol{I} = \boldsymbol{P}\boldsymbol{I}_s. \tag{15}$$

The remaining quantities defined in (14) and (15) are calculated in terms of surface integrals. Such equations represent the enforcement of Kirchhoff voltage and current laws and lead to the same set of (11), where the surface impedances substitute the volume resistances:

$$\begin{bmatrix} -\boldsymbol{A} & -\left(\hat{\boldsymbol{Z}} + j\omega\boldsymbol{L}p\right) \\ j\omega\boldsymbol{U} + \boldsymbol{P}\boldsymbol{Y}_{le} & -\boldsymbol{P}\boldsymbol{A}^t \end{bmatrix} \begin{bmatrix} \boldsymbol{\Phi} \\ \boldsymbol{I} \end{bmatrix} = \begin{bmatrix} \boldsymbol{V}_s \\ \boldsymbol{P}\boldsymbol{I}_s \end{bmatrix}. \tag{16}$$

B. Scaling

The system of (16) is typically an ill-conditioned problem because charges are usually much smaller than currents and voltages. Correspondingly, the entries of the matrix $\boldsymbol{P}$ are larger than other elements in (16) by several orders of magnitude. The ill conditioning of (16) makes the use of iterative as well as direct solvers more problematic and prevents to achieve the required accuracy. In order to mitigate such a problem, scaling can be adopted. The units of the electrical quantities will be therefore changed consistently as shown in Table I.

TABLE I
SCALING COEFFICIENTS

Voltage	V	C	pF
Current	mA	R	kΩ
Charge	pC	Lp	μH
P	pF^{-1}	f	GHz

The scaling factors have to be chosen in order to make more uniform as possible the magnitude of the matrix elements in (16). The choice of the scaling coefficients is not obviously unique. The selected coefficients in Table I have been found the most convenient for the problem under analysis. Other fields of applications may require different choices of the scaling factors.

[1] $\boldsymbol{R}$ is rigorously diagonal only for a given selection of the discretization structure; in general it is only "quasi-diagonal," i.e., it is a banded matrix.

C. DC Solution in PEEC

To have a better insight of the dc solution, it is useful to remind that in PEEC modeling, the reference node of the equivalent circuit is assumed to be at infinity.

At dc, a total decoupling of electric and magnetic fields occurs. Equations (14) and (15) are to be solved setting $\omega = 0$, and it has to be considered that the number of nodes of the equivalent circuit is decreased by one since there is no connection to infinity anymore.

This means that a node among those resulting from the discretization process is to be chosen as reference node. A reduced connectivity matrix $\boldsymbol{A}_r$ can be generated for the reduced circuit at dc and (16) become

$$\begin{bmatrix} -\boldsymbol{A}_r & -\boldsymbol{R} \\ \boldsymbol{0} & -\boldsymbol{A}_r^t \end{bmatrix} \begin{bmatrix} \boldsymbol{\Phi}_r \\ \boldsymbol{I} \end{bmatrix} = \begin{bmatrix} \boldsymbol{V}_s \\ \boldsymbol{I}_{sr} \end{bmatrix}. \tag{17}$$

In case the structure consists of conductors which are not directly connected (absence of a dc path connecting them), (17) needs to be solved for each of them, separately. Equation (17) can be solved for the unknown potentials $\boldsymbol{\Phi}_r$ and currents $\boldsymbol{I}$ as

$$\boldsymbol{\Phi}_r = \left(\boldsymbol{A}_r^t \boldsymbol{R}^{-1} \boldsymbol{A}_r\right)^{-1} \left(\boldsymbol{I}_{sr} - \boldsymbol{A}_r^t \boldsymbol{R}^{-1} \boldsymbol{V}_s\right) \tag{18a}$$

$$\boldsymbol{I} = \boldsymbol{R}^{-1} \left(-\boldsymbol{A}_r \boldsymbol{\Phi}_r - \boldsymbol{V}_s\right). \tag{18b}$$

Hence, the strategy to obtain the solution, from dc to the maximum frequency of interest, will be based on (16) for $\omega \neq 0$ and (17) for the dc.

D. Skin Effect Modeling

The surface formulation of PEEC is based on the equation $Z_s \boldsymbol{J}_s = \boldsymbol{E}_{\tan}$, where $\boldsymbol{J}_s$ is the equivalent current on the surface of the conductor and $\boldsymbol{E}_{\tan}$ is the vector component of electric field which is tangent to the surface.

The methodology used for the computation of the effective surface impedance $Z_s^{\text{eff}}(\boldsymbol{r})$ is presented in [27]. For the purpose of developing the effective surface impedance, we restrict our analysis to the case where the current flow inside the conductor is axial. Basically, the surface impedance is computed by evaluating the tangential electric and magnetic field on the surface of the conductor, thus allowing to identify $\boldsymbol{E}_{\tan}$ and $\boldsymbol{J}_s$ and, thus, $Z_s^{\text{eff}}(\boldsymbol{r})$.

Even though evaluated for the case of an axial current flow in the conductor, the effective surface impedance is applied to both tangential components of the electric field on the conductor surface.

E. Linear System Solution Methods

The linear system (16)—or (17) for the dc case—can be solved by using direct or iterative solvers. In case of iterative solvers, an acceleration technique can be used to efficiently evaluate the product between vectors and the not sparse matrices appearing in the PEEC formulation. It is, however, worth noting that ALEEN structures can contain a large number of terminals (see Section IV) leading to a very high number of solutions to evaluate. This can completely annihilate the saving in terms of CPU time obtained by the acceleration algorithm, and this is the case for the mock-up. In case of a large number of ports, we can exploit the saving on the dynamic memory obtained with accelerated iterative solvers to analyse models larger than the maximum allowable byte use of a direct solver. So, for the cases like the mock-up considered in Section IV, the use of a direct solver is recommended. Also the use of out-of-core implementations can be useful.

F. Acceleration Technique

If N indicates the number of unknowns, the solution of the S-PEEC linear system by a direct method (matrix inversion) employs $O(N^3)$ CPU time and $O(N^2)$ memory. In case we use an iterative solver (and a reliable preconditioner) the CPU time reduce to $O(N^2)$. Acceleration techniques, like the Multilevel Fast Multipole Method (MLFMA) or the adaptive cross-approximation (ACA) [26] can be used to evaluate, in a computationally efficient way, the matrix-vector product needed by the iterative solver. Such techniques typically reduce the memory and CPU requirements to $O(N\log_2 N)$.

In the S-PEEC linear system, two dense matrix-vector products are required: $\boldsymbol{L}p\boldsymbol{I}$, $\boldsymbol{P}(\boldsymbol{A}^t\boldsymbol{I})$. An acceleration technique will be applied on these matrices, being all the other matrix-vector products involve diagonal or sparse matrices.

In the frequency range of interest, the structure under analysis is electrically small. In such a case, the ACA allows representing the full submatrices of the S-PEEC linear system in a very efficient way.

The ACA algorithm is based on the fact that an impedance matrix of rank $m \times n$ related to two well-separated blocks of basis functions can be approximated by the product of two matrices of rank $m \times r$ and $r \times n$, with $r < \min(m,n)$, respectively. Hence, we can store only $(m+n) \times r$ matrix elements instead of $m \times n$. The algorithm is purely algebraic, and it can be used in all the frequency range down to $f = 0$, resulting in $O(N\log_2 N)$ complexity [26].

The main drawback in the analysis of an ALEEN structure is due to the fact that the linear system has to be solved for each one of the excitation configurations needed to provide the ALEEN external characterization. As stressed in Section IV, the usually large number of terminals can completely vanish the CPU time saving obtained by the acceleration method. Unless a very reliable preconditioner is used, a direct solver can be more convenient for the full characterization of the ALEEN structure. The mock-up considered in Section IV has been analyzed by a direct solver.

G. Impedance Matrix Characterization of ALEEN

The ALEEN has to be represented from the point of view of its ground terminals, each located generally close to the open-side terminals of the 3-D EWIS pathways. Such representation has to assure a complete external characterization of ALEEN, and it should easily interface with an external electrical database for a subsequent circuital modeling of EWIS.

By considering the ALEEN structure as a multiterminal network, its natural representation is given by the canonical

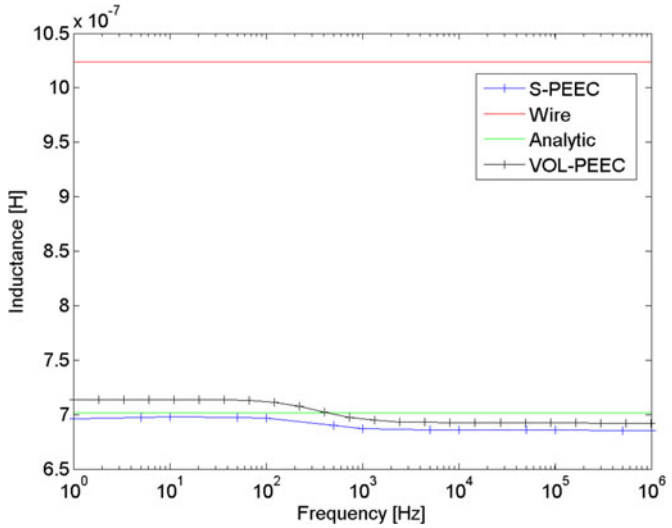

Fig. 1. Inductance of the rectangular bar obtained by means analytical formula (green), PEEC surface formulation (blue), and PEEC volumetric formulation (black). The inductance of a cylinder having the same dc resistance is also shown (red).

impedance $\boldsymbol{Z}$ or the canonical admittance $\boldsymbol{Y}$ matrices, with a reference node located at infinity.

By considering that ALEEN will be employed connecting loads and generators to a couple of terminals, a convenient representation is obtained by the evaluation of the impedance (self and mutual) between each couple of terminals

$$z_{ij,pq} = \left.\frac{V_{i,j}}{I_{p,q}}\right|_{I_{m\,,n}=0, m\,,n\neq p,q} \tag{19}$$

which can be easily interfaced with a circuital model of the ALEEN/EWIS whole system. It is worth noting that this is a redundant representation. As observed in Section IV, we can evaluate it from a minimum set of impedances (also the use of a reference terminal as reference is possible).

H. High-Fidelity Modeling

The combination of canonical shapes (like cylinders, bars, etc.) is often used to model the real structure under analysis [28] adopting a low-fidelity modeling approach. At one hand, this allows the use of analytical formulas to filling the linear system to be solved. On the other hand, some approximations are unavoidably inserted into the electromagnetic model, not allowing accurate modeling of the real structure, especially taking into account the need of considering very large relative frequency bands. As basic example, if we model a rectangular bar (length $L = 1$ m, width $W = 10$ cm, thickness $T = 1$ mm) with a cylinder and set the dimension in order to reproduce the same dc resistance a significant error in the reactance occurs, as shown in Fig. 1.

This simple test clearly shows the necessity to use high-fidelity models rather than low-fidelity ones. The evaluation of the geometrical and electrical parameters of canonical geometries in order to reproduce accurately the resistance, skin effect, and internal and total inductances of complex shapes—when possible—is not an easy task and only high-fidelity models provide sufficient accuracy to make useful the numerical model. Moreover, following a high-fidelity approach, the geometry imported form CAD files can be directly used, and no more work is required to the user.

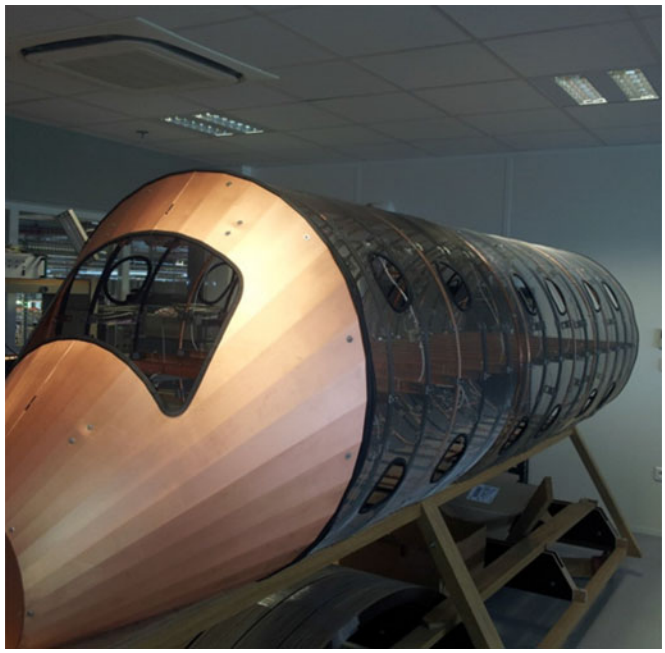

Fig. 2. Physical mock-up.

III. Description of the Mock-Up

The performances of the S-PEEC method and the whole tool [29] were validated against impedance measurements performed on a physical mock-up. This section describes the physical and the numerical mock-ups realized for this purpose.

A. Physical Mock-Up

The designed and realized mock-up is a complex object, representative for a complex composite aeronautical environment. A CAD model was created and used as an input both for the construction of the physical mock-up and the numerical mock-up.

The complexity of the object designed lies in the diversity of materials used and their respective impedances, cross sections of chosen elements versus volume, shapes, and number of connections and connected elements. The mock-up overall picture is presented in Fig. 2, while Fig. 3 presents some of its components.

The mock-up is composed of two main parts:

1) EWIS—four cable harnesses installed inside the mock-up, including the end fittings (lugs, male/female contacts);
2) ALEEN—composed of all the structure conductive elements that are electrically connected (i.e., aircraft nose, fuselage expanded foil, crossbars, some cables, connectivity elements, fixation elements, and conductive cable pathways.

Most of the elements are made in annealed copper with a mean resistivity of 1.84×10^{-8} Ω·m: copper tubes for the frames,

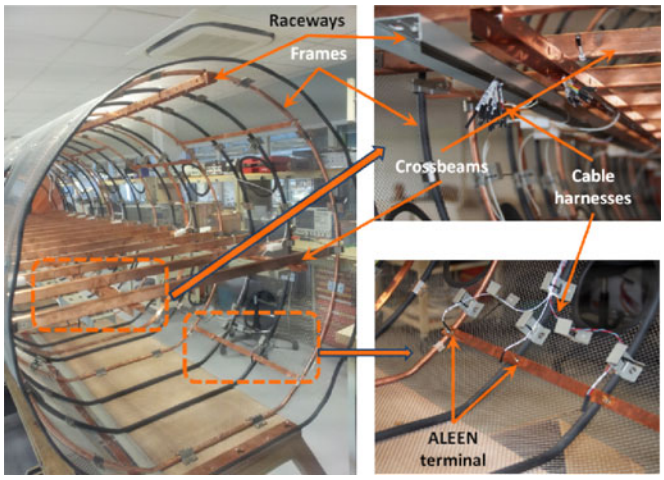

Fig. 3. Elements of the mock-up.

U-shape copper bars for the crossbeams and raceways. The fuselage is made of non magnetic steel expanded foil, having a square surface impedance of 10 mΩ in the frequency band of interest (dc–1 MHz). One hundred eighty connections between structural elements are made using complex fixation parts made of steel. Approximately, 300 steel screws are also used for connecting different parts: raceways and crossbeams, copper strips, frames, and expanded foil. Several test samples were created in order to characterize the mean contact resistances appearing between all these conductive elements, and the values obtained varied from 0.01 mΩ for a simple plane surface connection between a crossbeam and a raceway up to 3 mΩ for a complex connection between a crossbeam, a frame and the expanded foil.

Two of the harnesses placed inside the mock-up have AWG12 gauge cables, and the other two contain AWG18 gauge cables. For each gauge, the harnesses are placed in copper raceways on one side of the mock-up or in plastic raceways on the other side, thus allowing the comparison of impedances of loops created using similar cables but different current return paths.

B. Numerical Mock-Up

A "high-fidelity" numerical model of the mock-up was created and discretized in order to be analyzed with the S-PEEC method. The comparison between the electrical measurements carried out on the physical mock-up, and the corresponding results obtained from the electromagnetic simulations have been used to validate the ALEEN Modelling Tool [29].

The numerical model of the mock-up was built maintaining all the parts included in the real mock-up ("high-fidelity" model). For the frequency range of interest, the classical "lambda tenth" rule of thumb about the mesh size is obviously not applicable. In this case the mesh size was chosen in order to correctly model the real geometry.

Also, wire models of all the cables were included into the numerical mock-up, just having the requirements to fall in the 3-D harness pathways. Such cables, representing the EWIS, have been connected to the ALEEN in order to arrange the loops measured in the real mock-up. The numerical model of

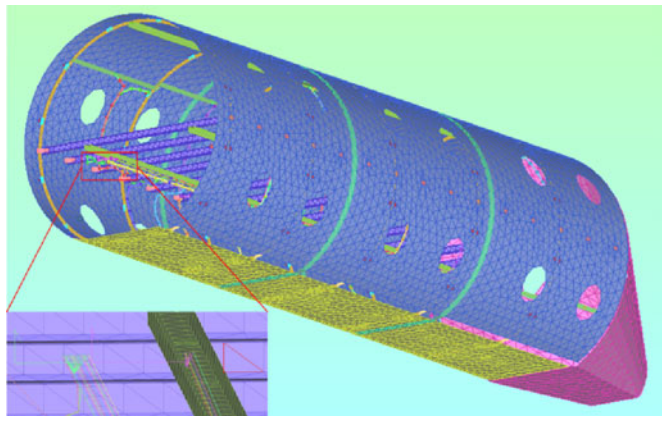

Fig. 4. Image of the numerical mock-up (mesh). The inset shows a particular of one side of two harnesses.

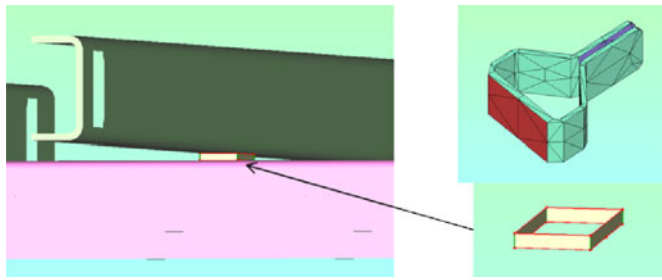

Fig. 5. Image of structural elements acting contact resistance.

the mock-up is shown in Fig. 4. The expanded foil constituting the fuselage can be assimilated to a thin plate with this resistance while there is no skin effect, in the frequency range dc–1 MHz.

The resulting model is made by 45 014 triangular elements and 1756 linear segments, with a mesh size varying from 1 to 6 cm.

The electrical characteristics (i.e., conductivity, surface impedance, and contact resistances) of the different parts were set on the basis of measurements on mock-up samples. The material characteristics can be specified in two ways: by conductivity and thickness of the material and by directly specifying the surface impedance. In both these cases, the values can be tabulated versus the frequency. At last, in case a part is geometrically thin and a meshed open surface is used, the values are obviously preprocessed in order to correctly represent the dc resistance and the skin effect.

The contact resistance between the different parts was taken into account by inserting small structural elements having appropriate surface impedance or by adjusting the surface impedance value of the fixation elements (see Fig. 5).

The electromagnetic model of the mock-up (comprising ALEEN and EWIS) has been simulated in the frequency range between 1 Hz and 500 kHz, obtaining the impedance of all the measurement loops. A set of terminals (points or portions of surface where we can inject or collect an external current $\boldsymbol{I_s}$) was defined on the ground terminals of ALEEN and on the open-side terminals of the 3-D EWIS pathways. The impedances have been compared to the measured ones in order to assess the accuracy of the formulation and of the applied models.

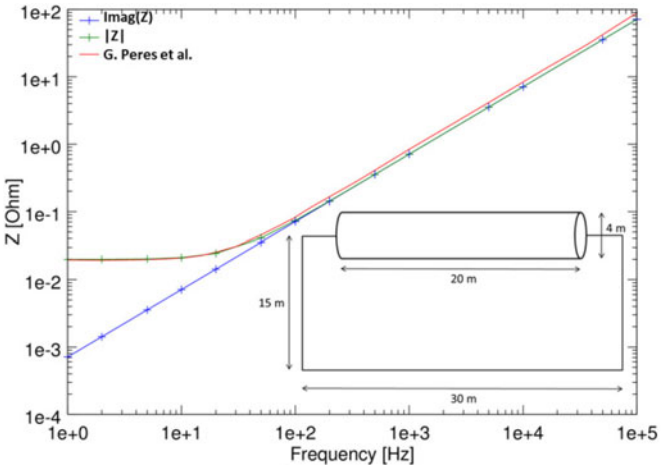

Fig. 6. Reactance (blue) and impedance (green) of the large cylinder shown in the inset. Data from [28] are also included (red).

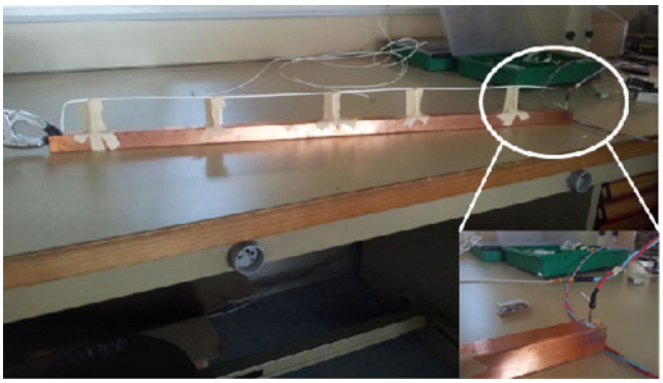

Fig. 7. Test sample used in validation. The 12 AWG cable is placed 5 cm over a copper U bar. The inset shows the two terminals of the loop.

IV. Measurements and Comparison with Numerical Results

The formulation was validated in two steps. At first, some preliminary tests were carried out by comparison with literature results and measurements on simple test cases. Then, the mock-up was simulated and the loop impedances were compared with the corresponding measurements.

The preliminary tests have included the large cylinder reported in [28]. The simulated reactance and the impedance are shown in Fig. 6 (the inset reports the geometry of the structure, where a delta-gap voltage source is placed in the middle of the loop), and they are in good agreement with the reference results.

The preliminary tests have also included the structure shown in Fig. 7. A 1 m long AWG12 cable was placed on top of a copper U-shape bar (with the following dimensions: 2 cm height, 1.5 cm width, and 1 mm thick) at a 5 cm distance. The cable was short-circuited with the bar on one side, as shown in Fig. 7. The inset in this figure shows the connection of the other terminals with the measurement cables. A calibrated measurement of the loop impedance was made using a HP 4194 A impedance meter. The measured and the simulated impedance are reported in Fig. 8, exhibiting a good agreement, except at low frequencies where we note some noise in the measurements.

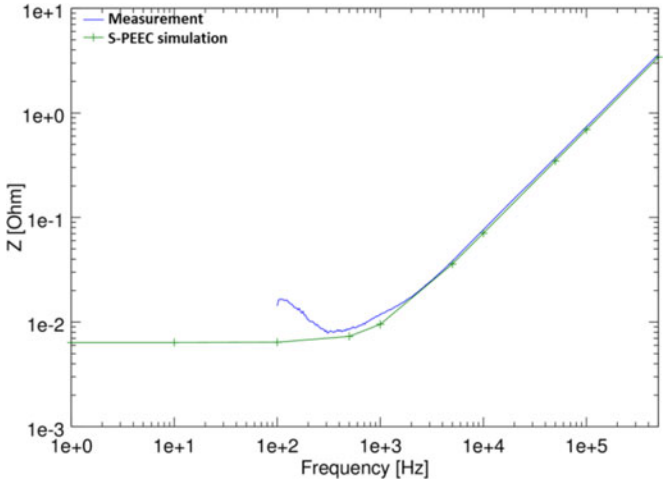

Fig. 8. Measured and simulated impedance of the test sample made by the cable over the U bar.

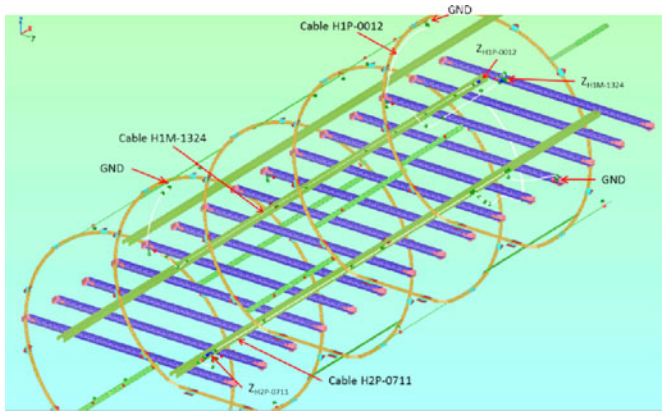

Fig. 9. Path of the three loops considered in Fig. 10. Cables are shown in white. GND indicates the connection point to the ALEEN structure. *Z* indicates the two terminals where the impedance is measured. The nose and the fuselage are not shown for clarity.

In the case of the mock-up, all the cables installed have the possibility to be connected (short-circuited) at one end to the mock-up structure, thus forming a loop that can be measured. All 38 measurement loops were measured one by one and simulated, and the results compared. The results corresponding to the three loops shown in Fig. 9 are shown in Fig. 10. The resulting impedances agree very well with measurements, confirming the accuracy of the S-PEEC formulation and the representativeness of the applied "high-fidelity" models.

In very few cases, a small difference in the reactance has been revealed. Following a deeper analysis of the physical mock-up configuration, it has been discovered that this is due to the presence of small loops formed by the wires, which were obviously not present into the CAD model (i.e., in the ideal cables layout), as in Fig. 11. Moreover, we observed a small difference in the resistive part at the highest frequencies of the band of interest. This is actually under investigation, but it results in a very low difference in the overall impedance.

It is worth noting that the use of terminals allows the evaluation of the impedance between any couple of terminals without the necessity of the insertion of feeding loops or others

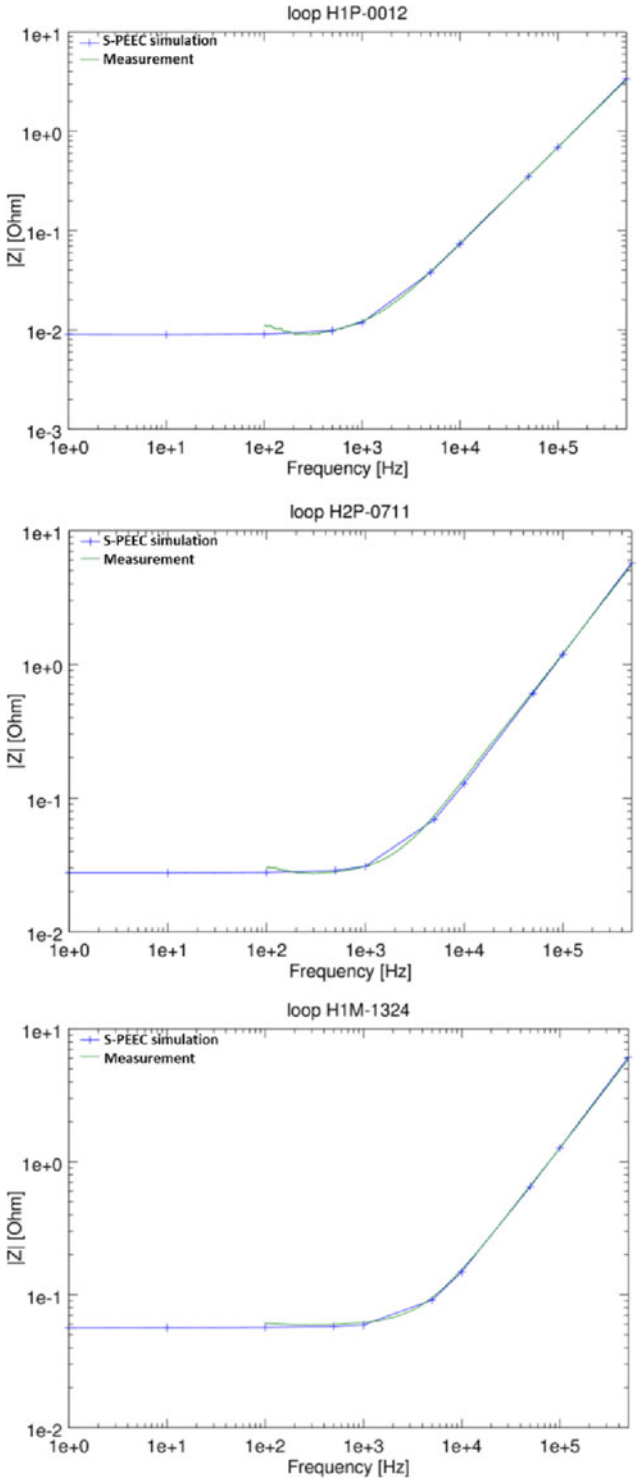

Fig. 10. Simulated and measured impedance (module) for three loops in different harnesses.

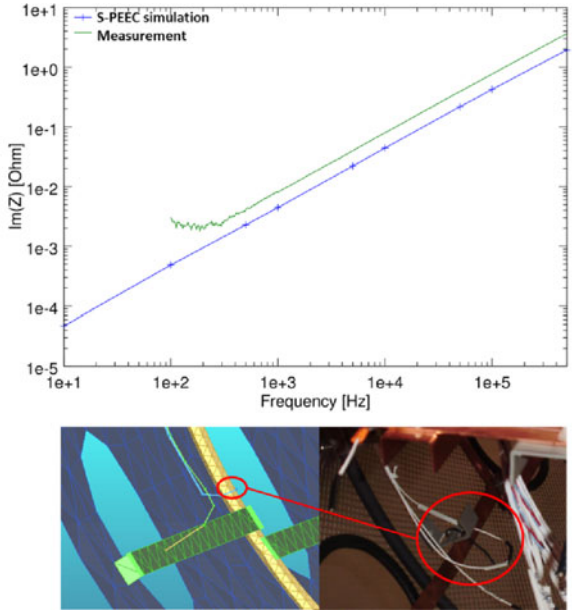

Fig. 11. Imaginary part of the impedance for a case with significant difference between measured (green) and simulated (blue) data. The difference is due to a loop not present in the numerical model (bottom).

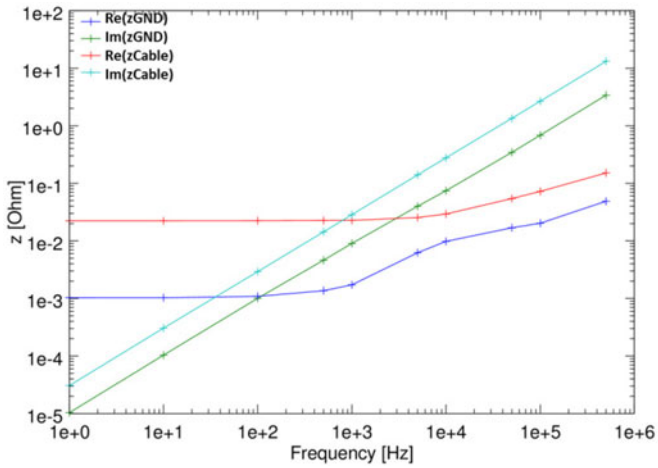

Fig. 12. Resistance and reactance of a cable and of ALEEN between the ground terminals of the cable itself.

fictitious structures which are needed when the classic concept of "port" is applied. In such a way, it is possible to evaluate an impedance representation of the ALEEN structure to be used in a subsequent verification or optimization step. Fig. 12 shows an example of the impedance of a cable and its relative ground terminals on ALEEN. Also the mutual impedance terms—not shown in the figure—between the cables and the ground terminals are evaluated in the simulation.

All the mock-up simulations were done by solving the S-PEEC linear system by a direct method. This required 99 GB RAM and 4:45 h for frequency on a 16 Intel Xeon Processor @ 2.90 GHz machine. A direct solver should be preferred in case of analysis of ALEEN structures, due to the high number of terminals (each one to be considered as a different excitation in order to evaluate the whole ALEEN Z-Matrix at terminals level): an iterative solver needs to solve the linear system for any couple of terminals, and the possible computational efficiency obtained by using an accelerating technique (MLFMA, ACA) can vanish.

In the mock-up, there are $M = 42$ terminals, leading to $M(M\text{-}1)/2 = 861$ different combinations. It is, however,

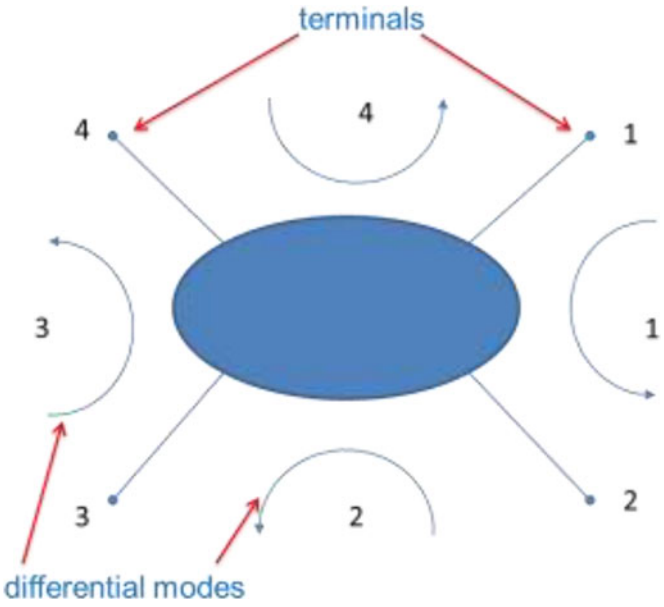

Fig. 13. Differential excitation constituting the minimum set of excitations needed to describe the structure.

possible to minimize the number of excitations to be analyzed by considering a set of differential excitations (in a number equal to the number of terminals) where contiguous terminals are excited (see Fig. 13). The impedances between any couple of terminals can then be evaluated by a simply linear combination of the terms relative to these solutions.

V. Conclusion

This paper presented an S-PEEC-based framework developed to model the current return networks installed aboard aircrafts having parts made in composite materials. A "high-fidelity" approach has been applied, which allows the simulation of real aircraft/ALEEN configurations with accuracy in the range of mΩ for impedances of ALEEN paths some meters longs. The electromagnetic model exactly reproduces the geometries of the structure under examination in order to accurately simulate both resistive and reactive effects (including skin effect) in the whole frequency range, through a single mesh model. Nominal and measured materials characteristics and bonding resistances of the contact points are used as input.

Acceleration techniques and effective preconditioners have been implemented in order to allow high-fidelity modeling also of large real-life aircrafts.

An unprecedented complex mock-up of a typical ALEEN structure, well representing real aircraft configurations, has been realized. A set of tens of measurements have been performed in the range dc–500 kHz and compared with the numerical results, showing very good agreement for the totality of cases and, therefore, validating the proposed numerical framework.

References

[1] A. E. Ruehli, "Inductance calculations in a complex integrated circuit environment," *IBM J. Res. Develop.*, vol. 16, pp. 470–481, Sep. 1972.

[2] A. E. Ruehli and P. A. Brennan, "Efficient capacitance calculations for three-dimensional multiconductor systems," *IEEE Trans. Microw. Theory Tech.*, vol. MTT-21, no. 2, pp. 76–82, Feb. 1973.

[3] A. E. Ruehli, "Equivalent circuit models for three dimensional multiconductor systems," *IEEE Trans. Microw. Theory Tech.*, vol. 22, no. 3, pp. 216–221, Mar. 1974.

[4] M. Li, M. A. Francavilla, F. Vipiana, G. Vecchi, Z. Fan, and R. Chen, "A doubly hierarchical MoM for high-fidelity modeling of multiscale structures," *IEEE Trans. Electromagn. Compat.*, vol. 56, no. 5, pp. 1103–1111, Oct. 2014.

[5] S. Arianos, M. A. Francavilla, M. Righero, F. Vipiana, P. Savi, S. Bertuol, M. Ridel, J.-P. Parmantier, L. Pisu, M. Bozzetti, and G. Vecchi, "Evaluation of the modeling of an EM illumination on an aircraft cable harness," *IEEE Trans. Electromagn. Compat.*, vol. 56, no. 4, pp. 844–853, Aug. 2014.

[6] A. E. Ruehli and H. Heeb, "Circuit models for three-dimensional geometries including dielectrics," *IEEE Trans. Microw. Theory Tech.*, vol. 40, no. 7, pp. 1507–1516, Jul. 1992.

[7] G. Antonini, A. Ruehli, and C. Yang, "PEEC modeling of dispersive and lossy dielectrics," *IEEE Trans. Adv. Packag.*, vol. 31, no. 4, pp. 768–782, Nov. 2008.

[8] G. Antonini, A. Ruehli, A. Mayo, J. Esch, J. Ekman, and A. Orlandi, "Non-orthogonal PEEC formulation for time and frequency domain EM and circuit modeling," *IEEE Trans. Electromagn. Compat.*, vol. 45, no. 2, pp. 167–176, May 2003.

[9] G. Antonini and A. Orlandi, "A wavelet based time domain solution for PEEC circuits," *IEEE Trans. Circuits Syst. I, Fundam. Theory Appl.*, vol. 47, no. 11, pp. 1634–1639, Nov. 2000.

[10] A. E. Ruehli and A. C. Cangellaris, "Progress in the methodologies for the electrical modeling of interconnects and electronic packages," *Proc. IEEE*, vol. 89, no. 5, pp. 740–771, May 2001.

[11] G. Antonini, M. Sabatini, and G. Miscione, "PEEC modeling of linear magnetic materials," in *Proc. IEEE Int. Symp. Electromagn. Compat.*, Aug. 18–22, 2006, Portland, Oregon, USA.

[12] G. Antonini, A. Orlandi, and A. Ruehli, "Analytical integration of quasi-static potential integrals of non-orthogonal coplanar quadrilaterals for the PEEC method," *IEEE Trans. Electromagn. Compat.*, vol. 44, no. 2, pp. 399–403, May 2002.

[13] G. Antonini and A. Ruehli, "Fast multipole and multi-function PEEC methods," *IEEE Trans. Mobile Comput.*, vol. 2, no. 4, pp. 288–298, Oct.–Dec. 2003.

[14] G. Antonini, "Fast multipole method for time domain PEEC analysis," *IEEE Trans. Mobile Comput.*, vol. 2, no. 4, pp. 275–287, Oct.–Dec. 2003.

[15] G. Antonini, D. Dischrijver, and T. Dhaene, "Broadband macromodels for retarded partial element equivalent circuit (rPEEC) method," *IEEE Trans. Electromagn. Compat.*, vol. 49, no. 1, pp. 35–48, Feb. 2007.

[16] G. Antonini, D. Deschrijver, and T. Dhaene, "Broadband rational macromodeling based on the adaptive frequency sampling algorithm and the partial element equivalent circuit method," *IEEE Trans. Electromagn. Compat.*, vol. 50, no. 1, pp. 128–137, Feb. 2008.

[17] F. Ferranti, G. Antonini, T. Dhaene, and L. Knockaert, "Guaranteed passive parameterized model order reduction of the partial element equivalent circuit (PEEC) method," *IEEE Trans. Electromagn. Compati.*, vol. 52, no. 4, pp. 974–984, 2010.

[18] F. Ferranti, G. Antonini, T. Dhaene, and L. Knockaert, "Passivity-preserving interpolation-based parameterized model order reduction of the partial element equivalent circuit (PEEC) method based on scattered grids," *Int. J. Numer. Modelling: Electron. Netw., Devices Fields*, vol. 24, no. 5, pp. 478–495, Dec. 2011.

[19] F. Ferranti, M. Nakhla, G. Antonini, T. Dhaene, L. Knockaert, and A. E. Ruehli, "Multipoint full-wave model order reduction for delayed PEEC models with large delays," *IEEE Trans. Electromagn. Compat.*, vol. 53, no. 3, pp. 243–248, Nov. 2011.

[20] G. Antonini and A. E. Ruehli, "Waveform relaxation time domain solver for subsystem arrays," *IEEE Trans. Adv. Packag. (Spec. Issue Recent Progress Elect. Modeling Simul. High-Speed Integr. Circuits Packages)*, vol. 33, no. 4, pp. 760–768, Nov. 2010.

[21] G. Antonini, D. Frigioni, and G. Miscione, "Hybrid formulation of the equation systems of the 3-D PEEC model based on graph algorithms," *IEEE Trans. Circuits Syst. I., Reg. Papers*, vol. 57, no. 1, pp. 249–261, Jan. 2010.

[22] F. Ferranti, G. Antonini, T. Dhaene, and L. Knockaert, "Guaranteed passive parameterized model order reduction of the partial element equivalent circuit (PEEC) method," *IEEE Trans. Electromagn. Compat.*, vol. 52, no. 4, pp. 974–984, Nov. 2010.

[23] G. Antonini, F. Ferranti, T. Dhaene, and L. Knockaert, "Physics-based passivity-preserving parameterized model order reduction for PEEC based analysis," *IEEE Trans. Compon. Packag. Manuf. Technol.*, vol. 1, no. 3, pp. 399–409, Mar. 2011.
[24] C. Ho, A. Ruehli, and P. Brennan, "The modified nodal approach to network analysis," *IEEE Trans. Circuits Syst.*, vol. 22, no. 6, pp. 504–509, Jun. 1975.
[25] S. M. Rao, D. R. Wilton, and A. W. Glisson, "Electromagnetic scattering by surfaces of arbitrary shape," *IEEE Trans. Antennas Propag.*, vol. AP-30, no. 3, pp. 409–418, May 1982.
[26] K. Zhao, M. N. Vouvakis, and J.-Fa Lee, "The adaptive cross approximation algorithm for accelerated method of moments computations of EMC problems," *IEEE Trans. Electromagn. Compat.*, vol. 47, no. 4, pp. 763–773, Nov. 2005.
[27] A. Rong, A. C. Cangellaris, and D. Limin, "Comprehensive broadband electromagnetic modeling of on-chip interconnects with a surface discretization-based generalized PEEC model," *IEEE Trans. Adv. Packag.*, vol. 28, no. 3, pp. 434–444, Aug. 2005.
[28] I. Revel, A. Piche, G. Peres, F. Flourens, C. Lochot, I. Terrasse, "Modeling strategy for functional current return in large CFRP structures for aircraft applications," in *Proc. IEEE Int. Symp. Electromagn. Compat.*, Sep. 8–12, 2008, pp. 1–5, EMC Europe.
[29] (Dec., 2014). [Online]. Available: http://genialproject.univaq.it
[30] (Dec., 2014). [Online]. Available: https://www.idscorporation.com/aeronautical/our-services-products/emi-emc-prediction-measurement/products/item/59-e-mind

Mauro Bandinelli was born in Italy in 1959. He received the Electronic Eng. Degree (*cum laude*) from the University of Florence, Florence, Italy.

He is currently with the "Electromagnetic Engineering Laboratory" and the "Space Laboratory," Ingegneria Dei Sistemi S.p.A., Pisa, Italy. He is currently involved in the development of numerical/asymptotic computational methods and CAE tools for electromagnetic modeling and in antenna and engineered materials design. He is the author or coauthor of about 90 papers at international meetings and on technical journals.

Mr. Bandinelli is the recipient of the Annual Italian Telecom Company award for his thesis work on "Numerical Methods for Antenna Array Design," in 1986.

Alessandro Mori received the Laurea degree (*cum laude*) in electronic engineering and the Ph.D. degree in telecommunication and information engineering from the University of Florence, Florence, Italy, in 1995 and 1998, respectively.

Until 2012, he was an External Collaborator with the Applied Electromagnetism Laboratory, Department of Electronics and Telecommunication, University of Florence. His current research interests include remote sensing and numerical methods in electromagnetics. He is currently with Ingegneria dei Sistemi S.p.A. (IDS), Pisa, Italy, where he is involved in research of computationally efficient full-wave methods for the analysis of electromagnetic scattering and radiation.

Giovanni Galgani was born in Italy in 1973. He received the Laurea degree (*summa cum laude*) in telecommunication engineering from the University of Siena, Siena, Italy, in 2001.

He has been an Electromagnetic Compatibility (EMC) Engineer and Antenna Designer with IDS Ingegneria dei Sistemi S.p.A, Pisa, Italy, since 2001. His current research interests include EM analysis of complex and large platforms and antenna design for avionic and space applications.

Daniele Romano was born in Campobasso, Italy, in 1984. He received the Laurea degree in computer science and automation engineering in 2012 from the Università degli Studi dell'Aquila, L'Aquila, Italy, where he is currently working toward the Ph.D. degree.

From July 2012 to July 2014, he was a Researcher at the UAq EMC Laboratory, Università degli Studi dell'Aquila, focusing on algorithm engineering and speed-up techniques applied to large EMC problems.

Giulio Antonini (M'94—SM'05) received the Laurea degree (*summa cum laude*) in electrical engineering from the Università degli Studi dell'Aquila, L'Aquila, Italy, in 1994, and the Ph.D. degree in electrical engineering from the University of Rome "Sapienza," Sapienza, Rome, in 1998.

Since 1998, he has been with the UAq EMC Laboratory, Università degli Studi dell'Aquila, where he is currently a Professor.

Anca-Lucia Goleanu Dieudonné received the electrical engineering degree from the "Politehnica" University of Timisoara, Timisoara, Romania, in 2007, the Research Master degree and the Ph.D. degrees in electrical engineering from the "Institut National Polytechnique de Grenoble," Grenoble, France, in 2008 and 2012, respectively.

She joined Labinal, Safran Group, in 2008, for the master internship. Since then she has been with the R&T Department, Labinal, today Labinal Power Systems, Safran Group. Her current research interests include low-frequency full-wave modeling aspects of electrical networks, current return networks in composite aircrafts, and optimization of large-scale systems in aeronautics.

Michel Dunand received the Advanced Technician Certificate of Physics from the "Ecole Nationale de Chimie Physique de Paris", Paris, France, in 1974. He has been with NEXANS to design optical fiber and microwave frequency cables. In 1991, he joined the R&D Department, LABINAL, to develop harnesses and their protection systems (electromagnetic, lightning, thermal, and mechanical). Since 2008, he has been a SAFRAN expert, where he is currently responsible of the Electrical Wiring Interconnection System (EWIS) upstream research and directly involved in the setting up and the achievement of several research programs.